G-JITTER EFFECTS ON NATURAL CONVECTION IN A CYLINDER A THREE-DIMENSIONAL NUMERICAL CALCULATION

T.Heiss, S.Schneider, J.Straub

Lehrstuhl A für Thermodynamik, Technische Universität München
Arcisstr.21, D-8000 München, West Germany

ABSTRACT

A numerical code has been developed to calculate three-dimensional natural convection in a cylinder. The numerical model is tested by comparison with experimental results: the onset of natural convection (critical Rayleigh number), velocity profiles in a horizontal cylinder and heat transfer in an inclined cylinder. Using this code the influences of g-jitter effects on natural convection were studied. The aim of this work is to demonstrate the increasing and decreasing natural convective fluid motion caused by gravity pulses of various amplitudes and durations. It can be shown that an increase in motion is proportional to the amplitude of the gravity pulse and the result of a rotating gravity vector is a decrease in motion with an accompanied increase in frequency.

Keywords: Microgravity, three-dimensional, numerical simulation, cylinder, natural convection, internal flow, heat transfer

1. INTRODUCTION

Buoyancy-driven instability and convective motion under microgravity in a differentially-heated geometry is of interest in material science experiments such as solidification of castings, purification of materials, growth of single crystals from melts, and many others. Kirchartz (Ref.1) carried out a numerical study of natural convective flow caused by gravity perturbations in a two-dimensional cavity. Because buoyancy-driven flow is mostly three-dimensional in real applications, we developed and tested a numerical code to investigate three-dimensionally onset of motion and internal flow. A cylindrical geometry was chosen to calculate buoyancy-driven flow caused by various microgravity perturbations such as gravity pulses and rotating gravity field.

2. ANALYSIS

2.1 Physical and mathematical model

The investigated problem is sketched in Fig.1.

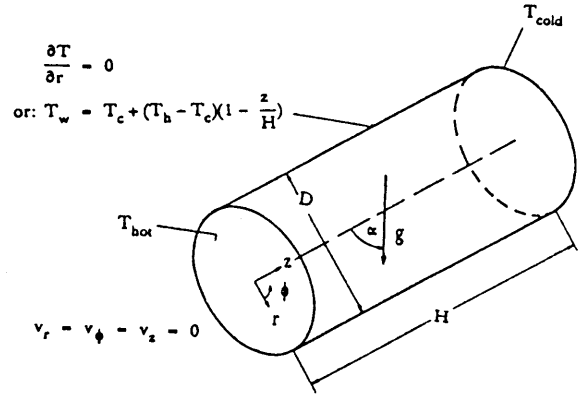

Figure 1: Schematic diagramm of the cylinder and the boundary conditions

The time-dependent, three-dimensional, buoyancy-driven flow in a gasfilled cylinder with constant properties except the density is governed by the following equations (compressive work and viscous dissipation neglected):

Proc. 6th European Symposium on Material Sciences under microgravity conditions, Bordeaux, France, 2-5 December 1986 (ESA SP-256, February 1987)

Equation of continuity

$$\frac{D\rho}{Dt} = -\rho(\nabla\vec{v}) \tag{1}$$

Equation of motion

$$\rho\frac{D\vec{v}}{Dt} = -\nabla p + \mu\nabla^2\vec{v} + \rho\vec{g} \tag{2}$$

Equation of energy

$$\rho c_p\frac{DT}{Dt} = k\nabla^2 T \tag{3}$$

Equation of state of an ideal gas

$$\rho = \frac{p}{RT} \tag{4}$$

with:

$$\frac{D}{Dt} = \frac{\partial}{\partial t} + v_r\frac{\partial}{\partial r} + \frac{v_\phi}{r}\frac{\partial}{\partial\phi} + v_z\frac{\partial}{\partial z}$$

$$\nabla = \frac{1}{r}\frac{\partial}{\partial r}r + \frac{1}{r}\frac{\partial}{\partial\phi} + \frac{\partial}{\partial z}$$

$$\nabla^2 = \frac{1}{r}\frac{\partial}{\partial r}\left(r\frac{\partial}{\partial r}\right) + \frac{1}{r^2}\frac{\partial^2}{\partial\phi^2} + \frac{\partial^2}{\partial z^2}$$

where ρ is the fluid density, $\vec{v}$ the velocity vector (v_r, v_ϕ, v_z), T the temperature, p the pressure, $\vec{g}$ the vector of gravitational acceleration (g_r, g_ϕ, g_z), μ the dynamic viscosity, k the thermal conductivity, c_p the specific heat and R the gas law constant.

We assumed non - slip conditions at all walls. The top and bottom walls are considered isothermal, the lateral wall either perfectly insulating or perfectly conducting.

$$T(r,\phi,0) = T_{hot} \tag{5}$$

$$T(r,\phi,H) = T_{cold} \tag{6}$$

perfectly conducting lateral wall:

$$T(R,\phi,z) = T_{cold} + (T_{hot} - T_{cold})(1 - \frac{z}{H}) \tag{7}$$

perfectly insulating lateral wall:

$$\frac{\partial T}{\partial r}\Big|_{r=R} = 0 \tag{8}$$

The aspect ratio (height - to - diameter ratio), the inclination angle α of the cylinder axis in the direction of the gravity field, the Prandtl number and the Rayleigh number are optionally varied. The following scales for non - dimensionalization are used:

Rayleigh number: $Ra = g\frac{\beta H^3 (T_{hot} - T_{cold})}{\nu\kappa}$

Prandtl number: $Pr = \frac{\nu}{\kappa}$

Fourier number: $Fo = t\frac{\kappa}{D^2}$

dimensionsless velocity: $\vec{v}^* = \vec{v}\frac{D}{\kappa}$

dimensionsless frequency: $f^* = f\frac{D^2}{\kappa}$

Where t is the time, ν is the kinematic viscosity and κ the thermal diffusivity.

2.2 Method of solution

Laminar natural convection inside a cylinder is studied by a three - dimensional time dependent calculation.

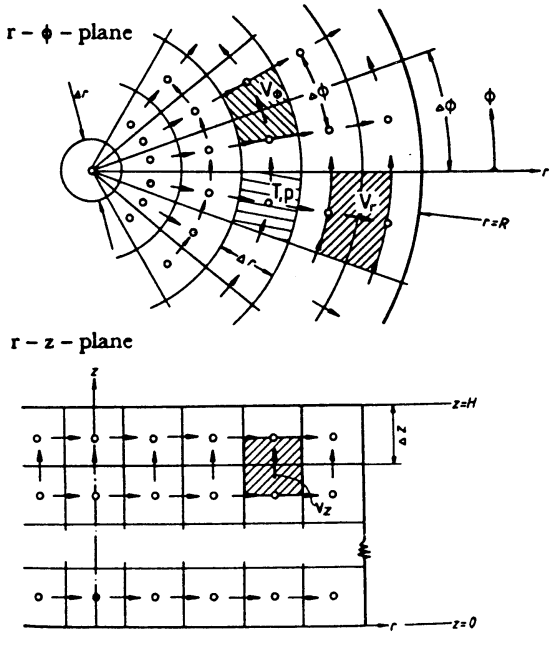

Figure 2: Grid arrangement in the r - ϕ - plane and r - z - plane

The numerical code is based upon a finite – volume method with explicit time steps and a semi – iterative pressure and velocity correction (Ref.2). The partial differential equations are discretisized by using an equidistant mesh (Δr = const., $\Delta\phi$ = const., Δz = const.).
The algebraic finite – difference equations are formulated in dimensional variables (v_r, v_ϕ, v_z, p, T). Temperature and pressure are defined in the center of the finite volumes. The velocities are calculated for points that lie on the faces of the control volumes ("staggered grid").
Fig.2 shows the grid arrangement and the locations of the velocity components in a radial and an axial cross – section. Exemplified a cylinder of aspect ratio one, the majority of the solutions reported in the paper were obtained with a 16*16*24 mesh, which was considered to represent a reasonable compromise between accuracy and computing cost. All properties except density, which is assumed to be depending on the temperature, are assumed to be time – independent and constant throughout the whole cylinder. The equation of state can be changed optionally for other fluids, such as liquid water or liquid metal.

2.3 Calculated results

In the case of a vertical cylinder ($\alpha = 0°$) with differentially heated end walls, the axial temperature gradient must exceed a certain value in order to start convective flow. This temperature gradient is characterized by the critical Rayleigh number Ra_{crit}. For $Ra < Ra_{crit}$ no convective flow is possible and heat transfer is only by conduction. For $Ra > Ra_{crit}$ a natural convection flow exists and there is conductive and convective heat transfer. A cylinder with a perfectly insulated lateral wall filled with an ideal gas ($Pr = 0.7$) is assumed. To obtain the critical Rayleigh number the fluid's reaction on a small temporary perturbation is studied. The initial conditions are no motion ($v_r = v_\phi = v_z = 0$) a linear temperature distribution from the bottom to the top ($\partial T/\partial z = (T_{cold} - T_{hot})/H$) and hydrostatic pressure distribution ($\partial p/\partial z = -\rho(T)g$). The convective flows are induced either by a temporary small inclination angle $\Delta\alpha = 0.2°$ ($H/D \geq 1$) or by an initial hot spot in the center of the bottom wall ($H/D \leq 0.5$) during the first time step (Fig.3). It can be shown that for $H/D \geq 1$ only a nonaxisymmetric flow state is stable and that for $H/D \leq 0.5$ a non – axisymmetric perturbation converts into a axissymmetric flow.

If $Ra < Ra_{crit}$ the perturbation is damped out, if $Ra > Ra_{crit}$ the maximal velocity increases again after the initial perturbation has faded out and reaches a finite steady state value after some time.

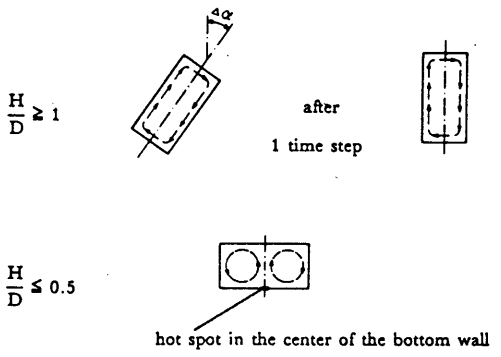

Figure 3: Small perturbation of the initial state of rest

Only in the case of the critical Rayleigh number is a steady state reached, after fading of the perturbation at which the velocities are very small (Fig.4). In Fig.5 the calculated critical Rayleigh numbers are compared with the theoretical results of Charlson, Sani (Ref.3) and the experimental results of Müller, Neumann, Weber (Ref.4).

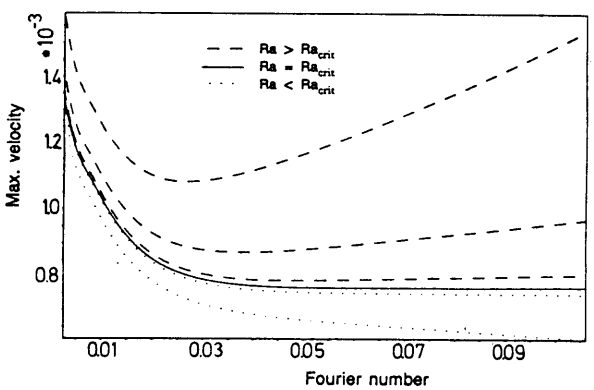

Figure 4: Determination of the critical Rayleigh number

Another test for our numerical code is the calculation of the velocity distribution measured by Schiroky, Rosenberger (Ref.5). Fig.6 shows the distribution of the axial velocity in the vertical midplane ($z = H/2$) of a horizontal cylinder ($\alpha = 90°$) with an aspect ratio of 5 and a perfectly conducting lateral wall.

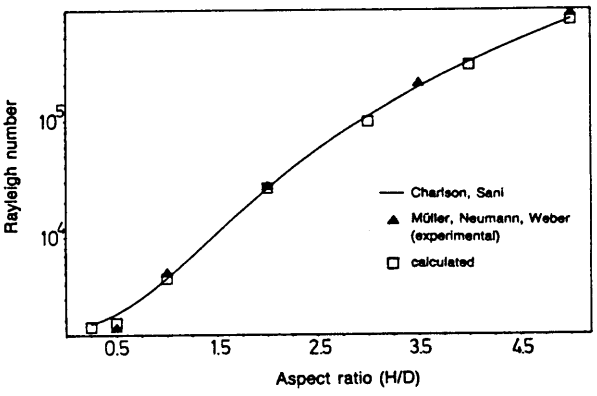

Figure 5: Critical Rayleigh number for different aspect ratios and a perfectly insulated lateral wall

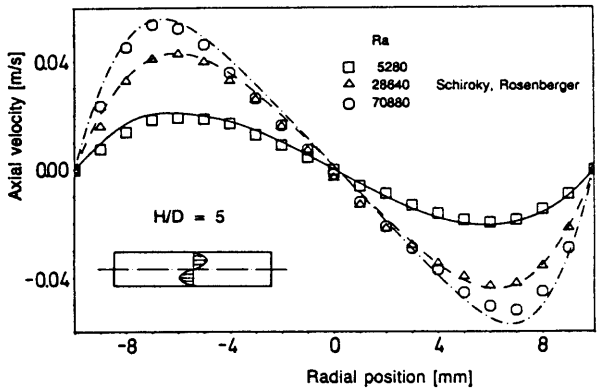

Figure 6: Axial velocity profiles in the vertical midplane (H/D = 5, $\alpha = 90°$)

3. EXPERIMENTS

An additional test of our numerical code could be a comparison of calculated and measured heat transfer from the hot wall to the cold wall inside an inclined cylinder. Because we didn't found any experimental results we constructed a test facility.

3.1 Apparature and instrumentation

The experimental apparatus is sketched in Fig.7. The cylinder (diameter 65 mm) is optionally filled with H_2, He or liquid water. The hot wall made of 6 mm thick copper is heated electrically by a thermofoil heater. It is thermally insulated by 6 mm of Teflon against the guard heater, which is also a thermofoil heater, and is placed in a copper tub. The temperature of the cold end wall made of 21 mm thick copper, is regulated by a water cooling system. The lateral wall of the cylinder is made of plexiglass and designed for pressures up to 6 bar.

Thus the Rayleigh number may be varied by changing the pressure and/or the difference of the temperatures between the heated and cooled end walls (upto $Ra/Ra_{crit} = 10^4$). Moreover, the aspect ratio (height – to – diameter ratio) can be varied from 0.5 to 5 and the inclination angle from 0 to 180 degrees. The entire cylinder is thermally insulated by Teflon plates at the end walls and styropor at the lateral wall.

To measure the temperatures, three thermocouples are installed in the cold wall, twelve in the lateral wall, four in the hot wall and two in the tub of the guard heater. The pressure is measured electrically as well.

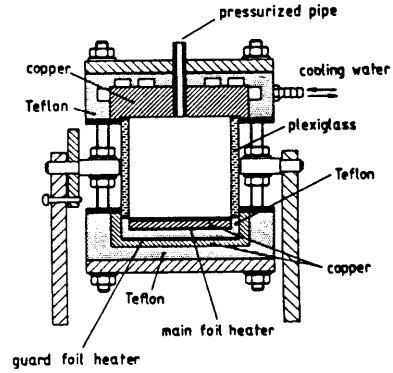

Figure 7: Experimental apparatus

A digital computer controls the experiment and stores the results. The thermocouples are scanned every 30 sec, the temperatures are calculated and the power supplies of the heaters are controlled by a digital PI – controller. If the steady state is reached, the heating power of the main heater is measured and recorded.

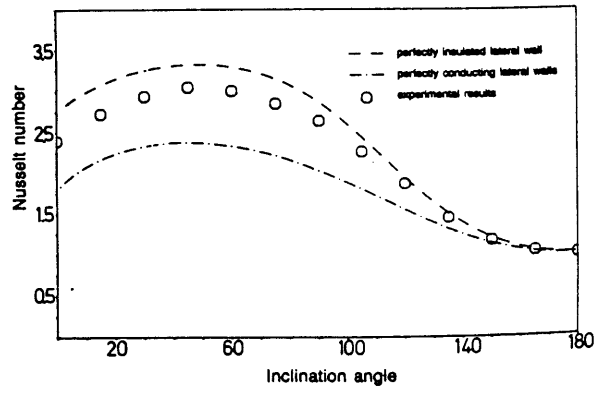

Figure 8: Calculated and measured Nusselt number of aspect ratio H/D = 1 and $Ra = 2 \cdot 10^4$

$$(Nu = \frac{\partial T}{\partial z}\Big|_{z=0} \frac{H}{T_{hot} - T_{cold}})$$

3.2 Experimental results

The results obtained in the experiment for $Ra = 2 \cdot 10^4$ and $Pr = 0.68$ (He) and various inclination angles α are compared with the numerical results for either a perfectly insulating or a perfectly conducting wall.
The experimentally obtained Nusselt numbers are found to lie between the theoretically predicted ones for a perfectly insulating and a perfectly conducting wall due to the test cells wall admittance (Fig.8).

4. CALCULATION OF G-JITTER EFFECTS

Starting from a state of rest (see section 2.3 except hydrostatic pressure distribution) single gravity pulses of various amplitudes (Rayleigh number Ra^*) and durations (Fourier number Fo^*) are applied to a gas-filled ($Pr = 0.7$) horizontal cylinder of aspect ratio one with a insulated lateral wall and differentially heated end walls (Fig.9). Figure 10a shows the development of the maximum velocity caused by a single gravity pulse of the nondimensional duration $Fo^* = 5.5 \cdot 10^{-3}$. During the gravity pulse the convective motion increases and reaches a maximum at the end of the gravity pulse. This maximum value depends on the nondimensional intensity Ra^* (Fig.10a), on the nondimensional pulse-duration Fo^* (Fig.11a) and on the aspect ratio H/D (Fig.12). It can be shown that the maximum value - Ra^* ratio is constant for the same aspect ratio. That means that all graphs in Figure 10a become only one graph if the maximum velocity is divided by the nondimensional intensity Ra^* of the pulse. In Figure 12 the dashed line (H/D = 1) includes all graphs of Figure 10a. Figure 10b shows the same graphs as Figure 10a but with a logarithmic scale, as can be seen from it the decay of the convective motion after the gravity pulse has vanished. For the studied range of Rayleigh number the decay constant is independent of the Rayleigh number Ra^*.

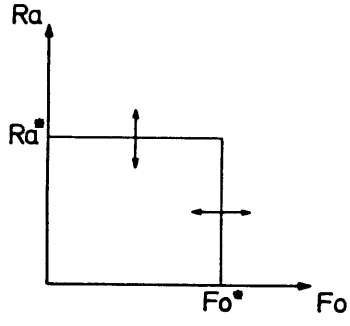

Figure 9: Gravity pulses with various amplitudes and pulse-durations

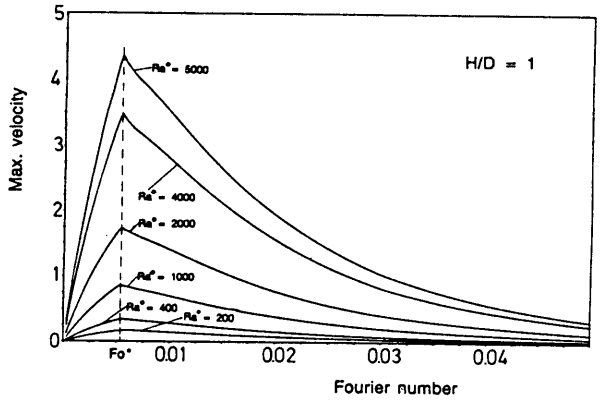

Figure 10a: Maximum velocity $\vec{v}^*$ caused by microgravity pulses of various amplitudes in a horizontal cylinder ($Fo^* = 5.5 \cdot 10^{-3}$)

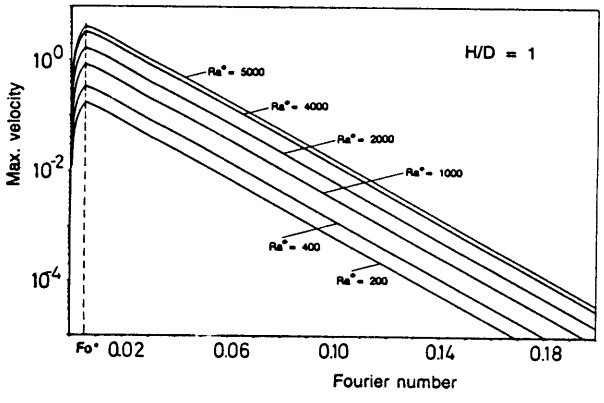

Figure 10b: Decay of convective motion (see Fig.10a)

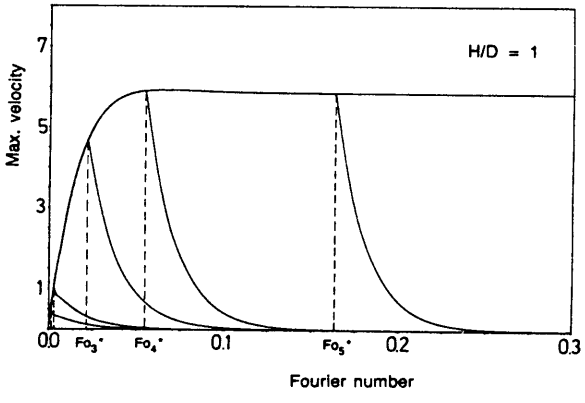

Figure 11a: Maximum velocity $\vec{v}^*$ caused by microgravity pulses of various pulse-durations in a horizontal cylinder ($Ra^* = 2000$)

Fig.11a and 11b show the influence of the pulse – duration Fo^* ($Ra^* = 2000$) on the maximum velocity. At the beginning of the gravity pulse the maximum velocity increases rapidly, overshoots at $Fo \approx 0.05$ and decreases slowly until the steady state is reached ($Fo \approx 0.15$). The overshot depends on the Prandtl number of the fluid and increases with decreasing Prandtl number (Ref.1). Fig.11a shows the time – dependent development of the maximum velocity for five various gravity pulses (nondimensional pulse – duration Fo^*). Figure 11b (the same graphs as Figure 11a but logarithmic scale) shows that the decay constant is independent on the pulse – duration Fo^* for a fixed aspect ratio as well.

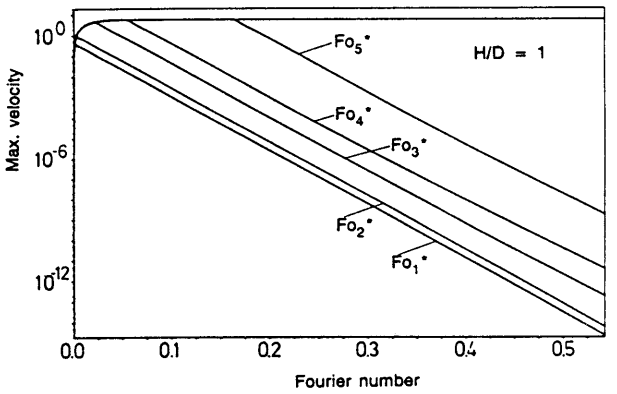

Figure 11b: Decay of convective motion (see Fig.11a)

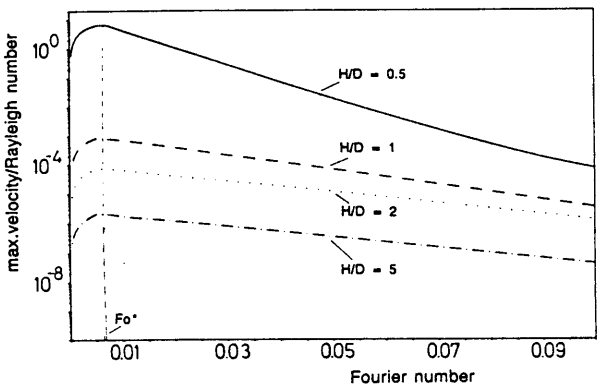

Figure 12: Maximum velocity $\vec{v}^*$ normalized by the amplitude of the gravity pulse Ra^*

Figure 12 shows the behavior of the maximum velocity for the nondimensional pulse – duration $Fo^* = 5.5 \cdot 10^{-3}$ divided by the nondimensional intensity Ra^* ($Ra^* = 0.5 Ra_{crit}$, see Fig.5). The aspect ratio H/D is varied from 0.5 to 5. The velocity – intensity ratio and the decay constant increase with decreasing aspect ratio.

The decay constant is independent on the intensity (Ra^*) and duration (Fo^*) of the gravity pulse and is only dependent on the aspect ratio.

Starting from a state of rest the steady state of the natural convective flow in a fixed cylinder is calculated for a rotating gravity field. Fig.13 shows the result of a gravity field rotating in the $r - \phi$ – plane on a horizontal cylinder of aspect ratio one, $Ra = 2000$ and with a perfectly insulated lateral walls. The nondimensional frequency f^* of the rotation is varied from 10^{-1} up to 10^3 step – by – step. It can be seen that up to a frequency $f^* \approx 10$ the steady state value of the maximum velocity is nearly the same as for a fixed gravity vector. If the frequency raises the maximum velocity decreases rapidly. A resonance frequency doesn't found.

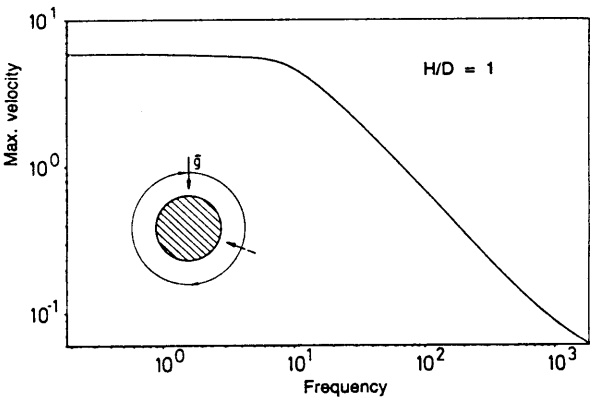

Figure 13: Gravity vector rotating at various frequences f^* in the $r - \phi$ – plane ($Ra = 2000$)

5. CONCLUSION

A numerical code was developed to calculate the three – dimensional, buoyancy – driven flow inside a cylinder with optional gravity conditions. The program is well – tested for the onset of convective motion and for laminar natural convection caused by a steady gravity field. The effects of gravity pulses and a rotating gravity vector is studied numerically. All computations are carried out for an ideal gas with $Pr = 0.7$. It is also possible to calculate internal flows in a cylinder filled with other fluids, such as liquid water or liquid metals. The gravity perturbations can be changed optionally. The interaction of natural convection and marangoni convection will be studied in the future.

6. REFERENCES

1. Kirchartz K R 1982, Thermische Konvektion als Folge zeitabhängiger Beschleunigungen, Spacelab – Nutzungen, *Status Seminar 1982 des Bundesministers für Forschung und Technologie*, 43 – 59

2. Pantakar S V 1980, *Numerical Heat Transfer and Fluid Flow*, McGrow Hill Book Company, Washington, New York, London

3. Charlson G S, Sani R L 1971, On thermoconvective instability in a bounded cylindrical fluid layer, *Int.J.Heat Mass Transfer*, Vol.14, 2157 – 2160

4. Müller G, Neumann G, Weber W 1984, Numerical Convection in Vertical Bridgman Configurations, *Journal of Crystal Growth*, Vol.70, 78 – 93

5. Schirocky G H, Rosenberger F 1984, Free convection of gases in a horizontal cylinder with differetially heated and walls, *Int.J.Mass Transfer*, Vol.27, 587 – 598